Colloids and Surfaces B: Biointerfaces 129 (2015) 47–53

Contents lists available at ScienceDirect

Colloids and Surfaces B: Biointerfaces

journal homepage: www.elsevier.com/locate/colsurfb

Wettability studies of topologically distinct titanium surfaces

Mukta Kulkarni[a,*], Yogita Patil-Sen[b], Ita Junkar[c], Chandrashekhar V. Kulkarni[b], Martina Lorenzetti[c], Aleš Iglič[a]

[a] Laboratory of Biophysics, Faculty of Electrical Engineering, University of Ljubljana, Tržaška 25, Ljubljana 1000, Slovenia
[b] Centre for Materials Science, School of Forensic and Investigative Sciences, University of Central Lancashire, Preston PR1 2HE, United Kingdom
[c] Jožef Stefan Institute, Jamova 39, Ljubljana 1000, Slovenia

ARTICLE INFO

Article history:
Received 28 November 2014
Received in revised form 22 February 2015
Accepted 9 March 2015
Available online 16 March 2015

Keywords:
Nanostructured titanium surfaces
Biomedical implants
Nanorough surfaces
Wettability
Surface electrochemical properties
Time-dependent contact area

ABSTRACT

Biomedical implants made of titanium-based materials are expected to have certain essential features including high bone-to-implant contact and optimum osteointegration, which are often influenced by the surface topography and physicochemical properties of titanium surfaces. The surface structure in the nanoscale regime is presumed to alter/facilitate the protein binding, cell adhesion and proliferation, thereby reducing post-operative complications with increased lifespan of biomedical implants. The novelty of our TiO_2 nanostructures lies mainly in the high level control over their morphology and roughness by mere compositional change and optimisation of the experimental parameters. The present work focuses on the wetting behaviour of various nanostructured titanium surfaces towards water. Kinetics of contact area of water droplet on macroscopically flat, nanoporous and nanotubular titanium surface topologies was monitored under similar evaporation conditions. The contact area of the water droplet on hydrophobic titanium planar surface (foil) was found to decrease during evaporation, whereas the contact area of the droplet on hydrophobic nanorough titanium surfaces practically remained unaffected until the complete evaporation. This demonstrates that the surface morphology and roughness at the nanoscale level substantially affect the titanium dioxide surface–water droplet interaction, opposing to previous observations for microscale structured surfaces. The difference in surface topographic nanofeatures of nanostructured titanium surfaces could be correlated not only with the time-dependency of the contact area, but also with time-dependency of the contact angle and electrochemical properties of these surfaces.

1. Introduction

Titanium (Ti) and its alloys exhibit highly promising biomaterial properties including high biocompatibility, great tensile strength, high corrosion resistance [1] and have more resistance to the effects caused by fluids that are excreted or secreted from the human body. Owing to these outstanding properties, Ti alloys are widely used in biomedical applications, for instance, to produce/fabricate implants for hard tissue replacement [2–4]. In order to improve the interactions with the living bone [4], the so-called "osteointegration" or "osseointegration" process, the implant surface made from Ti and its alloys needs to be physically and/or chemically modified [5,6]. Speed, strength and degree of osteointegration depend mainly on the surface properties of implants, among which chemistry, physics, topography and wettability are known to be very crucial factors [4,7,8].

The adsorption of proteins and, later, the adhesion of cells are time dependent phenomena which happen in steps. The initial response when the material is inserted in the biological surroundings is the adsorption of water molecules to its surface, which happens just within the first few nanoseconds. The reason is simply the abundance of water in the body. Many molecules, including proteins are dissolved in the aqueous medium. Therefore, understanding the wetting behaviour and the wettability kinetics of the material surface with water becomes an essential step, which has been focused in the present work.

As an example, we checked the interaction of water droplet with nanostructured titanium surfaces. Surface roughness and surface physicochemical properties (among them wettability) of the biomaterial are interrelated with the protein adsorption phenomenon [9–11]. The water adsorption to the implant surface depends on the charge density of the surface which is strongly influenced by its nanoscale roughness [12,13]. These factors have the major

* Corresponding author. Tel.: +386 1 4768 235; fax: +386 1 4268 850.
E-mail address: mukta.kulkarni@fe.uni-lj.si (M. Kulkarni).

http://dx.doi.org/10.1016/j.colsurfb.2015.03.024
0927-7765/

contribution in defining the implant surface-to-blood interactions as well as influencing the cell adhesion and, consequently, their growth and differentiation [14–16]. After the initial adsorption of water molecules to the surface, the second stage involves the adsorption of proteins. Implant surfaces e.g. titanium dioxide (TiO_2) surfaces and cell membranes are both negatively charged [17]; it is therefore necessary to have a mediator that shields the repulsive force between them [17,18]. Proteins often work as these mediators thereby bridging the repulsive electrostatic interactions between equally charged surfaces [18]. First, small proteins get adsorbed, due to their rapid transport to the surface, which over time are partially replaced by bigger ones having greater affinity towards the surface [19], following the "Vroman effect" theory. The binding of bigger proteins is sometimes mediated by previously bounded smaller proteins [14]. Smaller proteins are also known to mediate the adhesion of cell glycocalyx (i.e. glycoprotein-polysaccharide cell coating) [17,18].

Surface properties, including wettability and charge, influence the adsorption of proteins which mediate the adhesion of bacteria and cells to the implant [7,8]. Some cells prefer to attach to hydrophilic surfaces, while others have characteristic attraction towards hydrophobic ones [20–22]. Generally, hydrophobic surfaces are considered to be more protein-absorbent than hydrophilic ones, due to the strong hydrophobic interactions [9,23]. However, this could cause conformational changes or, sometimes, denaturation of proteins and, thus, lower the proliferation of cells on such surfaces. It is reported that biomaterial surfaces with moderate hydrophilicity display improved cell growth and biocompatibility [13]. Nevertheless, cell adhesion can decrease as the material becomes too hydrophilic. Cell proliferation also depends on an appropriate orientation of proteins, which gives guidance to the cells. Time dependent conformational changes of adsorbed proteins as well as adhesion kinetics and strength of protein binding [9,24] are, therefore, of primary importance. Another key factor to tailor the biological response is the surface electric charge of the implant. Most of the plasma proteins are negatively charged at physiological pH (pH = 7.4), so that repulsive electrostatic interactions are expected to occur towards the negatively charged Ti-implant surface [17,18]. Once again, the protein conformational changes play an important role [25]. The optimisation of the physicochemical surface properties [17,18], in this manner, becomes a crucial parameter to be considered while designing the biomedical implants [26].

The surface topography considerably alters the cellular behaviour in terms of adhesion, spreading, migration, proliferation and signalling [7]. For instance, fibroblasts and epithelial cells adhere more strongly to smooth surfaces, whereas rough surfaces aid in osteoblastic proliferation and collagen synthesis [27]. In general, larger the effective (real) surface area, higher is the degree of bone-to-implant (BIC) contact, which is one of the important elements for the success of orthopaedic implants [28]. It should be also stressed that micro and nanoscale patterns are not only observed in implant substrates (in vitro) but are also seen in vivo, for example, fibrils and fibre bundles (collagen and fibrin) [29], rough surfaces (crystal deposit in bone) and porous membranes (basement membranes) [30]. These naturally occurring hierarchical patterns play an important role in many biological tissues, including bone, teeth, and cartilage [29,31] as their surface properties, such as wettability and topography (and their interdependence), determine the adhesion and proliferation of cells in biological systems [15,16,18,32]. Moreover, nanostructured surfaces are shown to play an important role in osteoblast proliferation as well as in mimicking natural bones [33–35]. In fact, cells are presumed to sense and respond to such nanoscale topographical attributes also through membrane deformation and stretching [18,36,37]. All these surfaces own a specific nanostructure which enables the desirable adsorption of proteins which further guide cells.

Within the biomedical community, the nanorough (1–100 nm) surfaces are becoming more popular than macro (10 μm to 1 mm) and micro (1–10 μm) rough surfaces. Nanoscale topography increases the effective (real) nanoscale surface area and, thus, enhances the ability to withstand more molecules, like proteins. Due to higher surface charge density at nanoscale sharp edges, nanoscale sharp edges may facilitate monovalent and divalent cation-mediated binding/adhesion of proteins to the surface [17,18]. The layer of the adsorbed proteins and other molecules, in this manner, improves the cell attachment to the surface [38]. In the current study, we have employed nanorough titanium dioxide surfaces, made of nanotubes and nanopores, and a microrough surface (titanium foil). The nanostructured surfaces were fabricated by electrochemical anodisation [39]. Parameters were tuned to obtain macroscopically flat, but locally rough nanoporous (15 nm pores) and nanotubular surfaces (diameters 50 and 100 nm). Studies demonstrate that the nanoscale morphologies display different wettability behaviour as compared to their microscale counterparts [40,41].

In general, the physics of liquid droplet interactions with nanostructured [40] and microstructured [41] surfaces have been the subject of increasing interest in the past few years. Most of the theoretical descriptions assumed that either the liquid drop penetrates into the surface invaginations (Wenzel regime) or the drop stays on the microstructured surface protrusions (Cassie regime) and does not contact the bottom plate [41]. Seldom, the intermediate situation is considered, where the drop partially protrudes into the invaginations of the microstructured surface, i.e. due to the roughness of the microscale protrusions on their top (Wenzel–Cassie regime) [41]. We show in this work that the TiO_2 nanostructures have a specific influence on the interaction between the water droplet and the surface. To some extent, this makes the droplet behaviour on TiO_2 nanotubular surface different from what expected on the microscale structured surfaces, based on the validity of either Wenzel or Cassie law. We propose that the specific behaviour of the nanostructured surfaces may have an important effect on the features that are crucial for designing orthopaedic implants, such as protein adsorption, cell adhesion and osteointegration. In addition, we measured the surface charge properties of the pristine and nanostructured titanium, to verify the occurrence of any variation in terms of isoelectric point (IEP) and zeta (ζ).

2. Experimental

2.1. Materials

Ti-foils of 0.1 mm thickness (99.6% purity) were obtained from Advent Research Materials, England. Distilled water used during the entire study was purified by Werner–Reverse osmosis equipment. Hydrofluoric acid (HF) and the solvents, namely Ethylene Glycol (EG), ethanol, and acetone, were purchased from Sigma–Aldrich, Germany and used without further purification.

2.2. Fabrication of TiO_2 surfaces

The Ti-nanostructures were fabricated according to the electrochemical anodisation method published earlier [1,39], although using slightly different parameters, as described below. Prior to anodisation, Ti-foils were degreased by successive ultrasonication steps in acetone, ethanol and deionised water for 5 min each and dried under the nitrogen stream. EG-based electrolytes were used to grow Ti-nanostructures with specific compositions, as listed in Table 1. All the anodisation experiments were carried out at

Table 1
Anodisation conditions used for fabrication of Ti-nanostructures.

Diameter of nanostructure	Electrolyte solution	Potential (V)	Time of anodisation (h)
Nanopores 15 nm	EG + 6 M water + 0.2 M HF	10	1
Nanotubes 50 nm	EG + 8 M water + 0.2 M HF	20	2.5
Nanotubes 100 nm	EG + 8 M water + 0.2 M HF	58	2.5

room temperature (~20 °C) in a two-electrode system, using the titanium foil as the working electrode and a platinum gauze as the counter electrode. As-formed nanostructures were allowed to stand in ethanol for 2 h in order to remove organic components from the electrolytic solution. This step was followed by washing of the nanostructures with distilled water and drying under nitrogen stream.

It should be stressed at this point that the hydrophobic/hydrophilic character of the TiO_2 nanopore/nanotube surface may depend on ageing, where the effect of ageing can be strongly modified/abolished by annealing or other methods [40,42,43]. For example by the aid of plasma treatment technique, the hydrophobic character of aged TiO_2 nanopore/nanotube surface will be reversed to hydrophilic, possibly due to the removal of surface contaminants, such as carbon. It was shown recently that wettability of TiO_2 nanosurfaces can change with time [41]. Keeping this in mind, in the current work we deliberately used 2-month-aged surfaces, which showed a hydrophobic (i.e. contact angle > 90°) or weakly hydrophilic character.

2.3. Atomic Force Microscopy (AFM)

Topographic features of Ti-foil and Ti-nanostructured surfaces were examined by Atomic Force Microscopy (Solver PRO, NT-MDT, Russia) in tapping mode in air. The samples were scanned with the standard Si cantilever at a constant force of 22 N/m and resonance frequency of 325 kHz (10 nm tip radius, 95 μm tip length). The average surface roughness (R_a) was calculated from $3 \times 3\ \mu m^2$ image areas. The results are shown as the average R_a from five different areas.

2.4. Scanning Electron Microscopy (SEM)

High contrast images of nanostructural morphology of Ti-surfaces were obtained by Scanning Electron Microscopy (Hitachi FE-SEM S4800). All samples were used without gold sputtering, as the untreated samples already display images with reasonably good contrast.

2.5. Contact distance (D) measurements

Water droplet contact areas, expressed in terms of contact diameter (D) of the curve fitted to the droplet image (see Figs. 3 and 5), on all the Ti-surfaces were measured at regular intervals using the Contact Angle Instrument (First Ten Ångstroms, Inc., USA, FTA1000 series). The measurement system consisted of a sample stage, vertically fitted Hamilton micro-syringe to place the water droplet on the sample and the camera mount – TV lens camera with Extension tube set 40 mm (Edmund optics, Japan). Images were captured and analysed for contact areas using the FTA32 Video 2.0 software. All the measurements were performed at room temperature (27 ± 1 °C).

2.6. Surface charge measurements by streaming potential

The surface charge analysis was accomplished using an electrokinetic analyser (SurPASS, Anton Paar GmbH, Austria). The pH dependence (titration curve) of *zeta potential* (ζ-potential) and *isoelectric point* (IEP) were obtained in 0.001 mol/L potassium chloride (KCl p.a., Carl Roth GmbH, Germany) solution by streaming potential measurements.

3. Results and discussion

3.1. Nanoscale morphology of Ti-surfaces

The morphological features of TiO_2 nanostructures were determined by SEM technique. High contrast images clearly define the dimensions of nanopores and nanotubes as shown in Fig. 1. SEM images demonstrate the nanostructural uniformity and hollowness of the surfaces as expected. The nanopores present an average diameter of 15 nm with standard deviation of 20%. Nanotubes samples have average 50 and 100 nm diameters with standard deviations of 10% and 5%, respectively.

The topographical features of the nanostructures investigated by AFM are shown in Fig. 2. The pristine (non-anodised) Ti-foil used for this study was flat at the macroscopic level, but presented local vertical distortions (vertical roughness) by AFM imaging at the microscopic level. The estimated vertical roughness of the Ti-foil was around 28 nm. Imaging of nanoporous Ti-surface (pore diameter of 15 nm) was not possible due to the excessive size of the AFM tip, which produced practical artefacts on the surface. The situation was almost similar for the Ti-surface with 50 nm nanotubes, which appeared to be closed rather than open (hollow) structures. This attribute was also reflected by a lower vertical roughness value (around 20 nm) as compared to the pristine Ti-foil. It was, however, possible to get better understanding of topographic features of Ti-nanotubes of 100 nm diameter as shown in Fig. 2. The AFM tip could penetrate the hollow into the 100 nm diameter nanotubes, providing a clear picture of the open nanotube structures. This was beneficial to validate the presence of nanotubes and their variable depth in contrast to two-dimensional SEM micrographs. The surface vertical roughness was estimated to be around 40 nm but the actual vertical roughness is presumed to be much higher, as the AFM tip could not distinguish the interstitial sites among the nanotubes and was not able to reach the bottom of the nanotube surface. Therefore, the AFM study revealed slightly different information than SEM, due to its technical limitations as described above.

3.2. Wettability studies of Ti-nanostructures by contact area kinetics

For each experiment, a single droplet of ~10 μl distilled water was placed on the Ti surface using the Hamilton micro-syringe. The images were captured immediately after placing the drop on the surface ($t = 0$) and every 5 min thereafter, until the complete evaporation of the drop. Fig. 3 displays images recorded after every 5 min until evaporation of the droplet (observed at 30 min). The largest planar distance between end points of a curve fitted to the side-view image of water droplet was defined as contact diameter D, which simply equals the diameter of the contact area (Figs. 3 and 5).

As expected [41], the D value for macroscopically flat and weakly hydrophilic Ti-foil changed significantly with time, especially in the later stages of evaporation, i.e. after 15 min (Fig. 4). The roughness of Ti-foil surface, albeit locally distorted and not ideally smooth

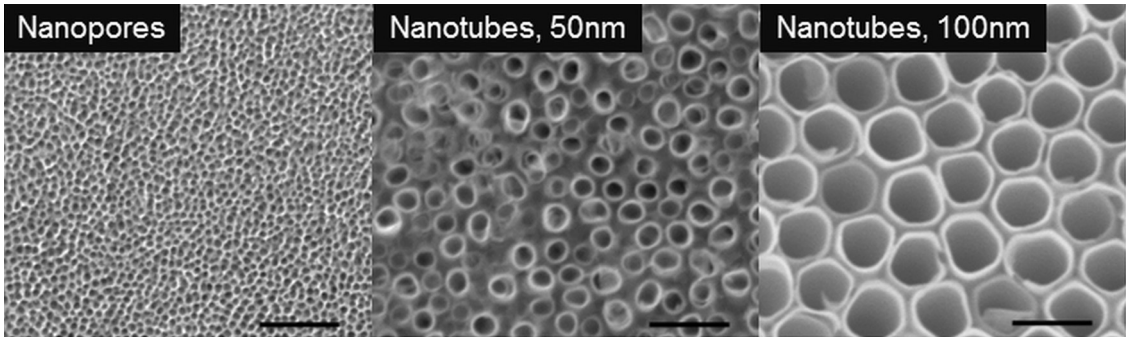

Fig. 1. SEM micrographs of Ti-nanostructures: Scanning Electron Microscopy images of titanium nanopores of diameter 15 nm, nanotubes of 50 nm and nanotubes of 100 nm diameter. Scale bar is 200 nm.

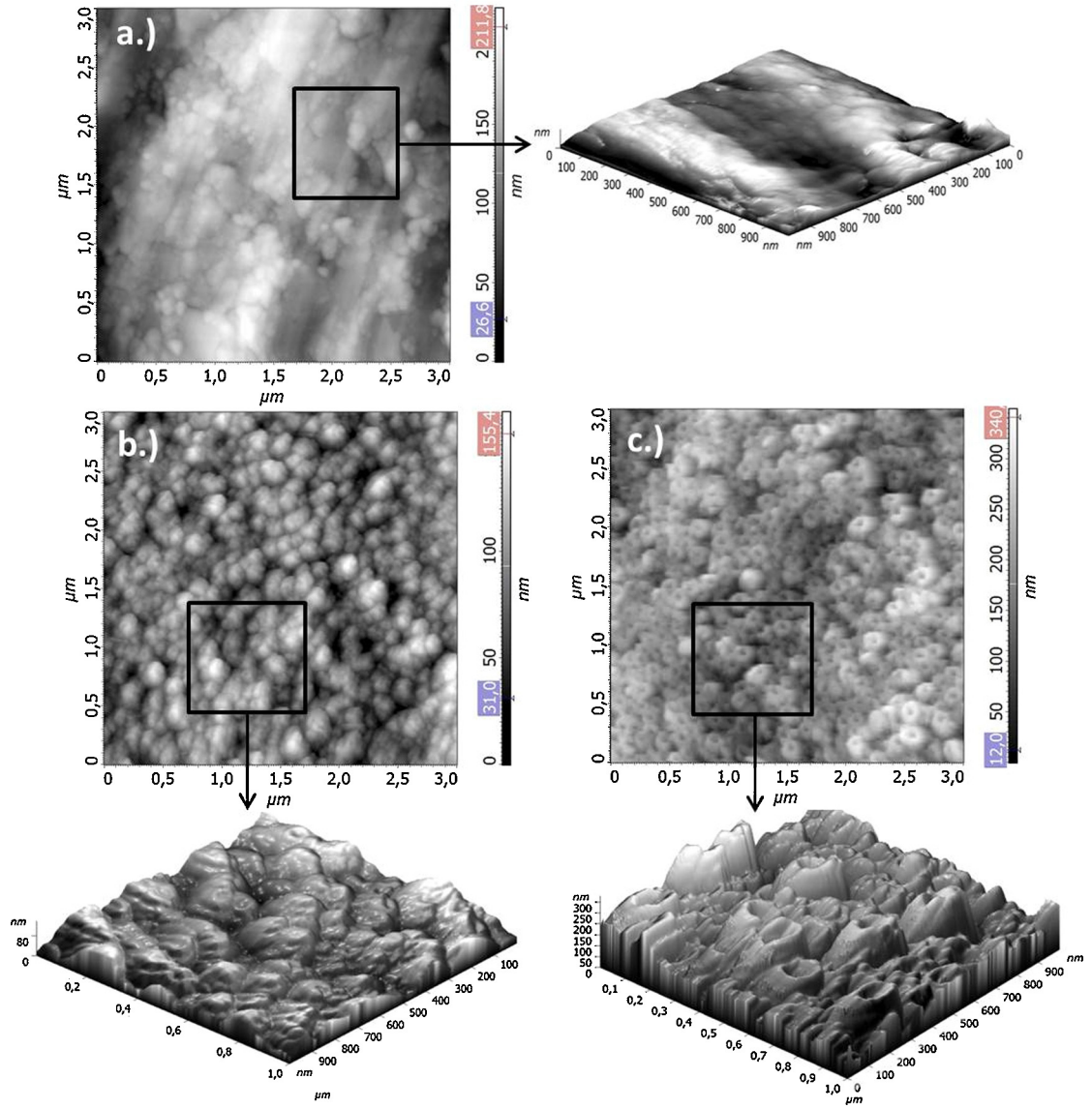

Fig. 2. AFM images of Ti-nanostructures: Atomic Force Microscopy images of titanium pristine foil, nanotubes of 50 nm and nanotubes of 100 nm diameter. Zoomed regions (along vertical 'z-direction') show further topological details.

[17], was not sufficient to hinder the receding of the droplet edge (contact line), i.e. to decrease the value of *D*. Therefore, the droplet evaporation after certain time [41], executed from the outer edges along 360°, caused the considerable decrease in the *D* value with time (see Fig. 4). In contrast, the nanoporous and nanotubular surfaces, due to their enhanced roughness (see Figs. 1 and 2), exhibited constant D values. This may be attributed to the penetration (at least partial) of the water into the hollow interiors of the nanopores/nanotubes and also into intermediate space among nanotubes (probably in accordance with mixed Wenzel–Cassie

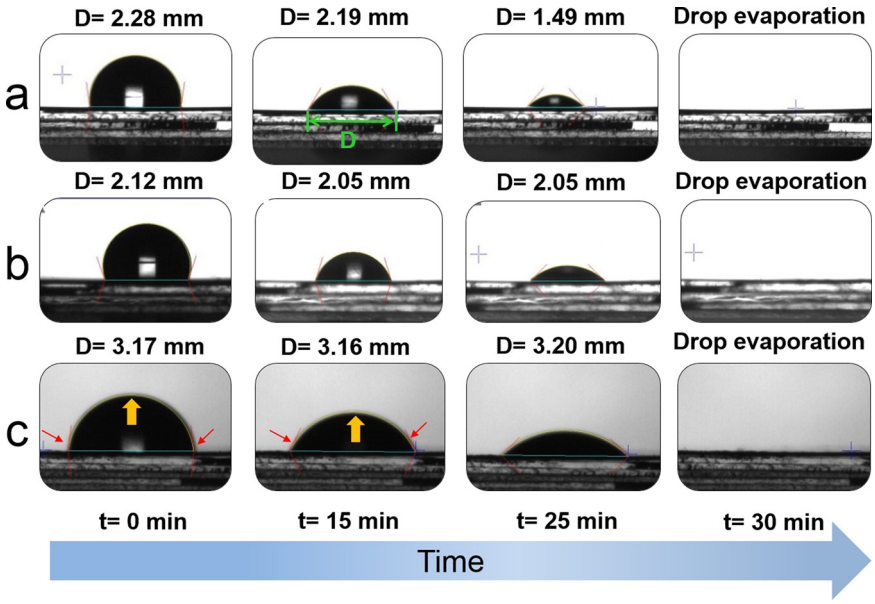

Fig. 3. Measurement of water droplet contact diameter with time: contact diameter of the contact area between the droplet and Ti-surface is depicted with *D* (measured in millimetres) for each surface as shown in (a) for pristine Ti-foil, (b) for TiO_2-nanotubes (50 nm diameter) and (c) for TiO_2-nanotubes (100 nm diameter). Red arrows were used to denote exact end points while yellow curves (e.g. yellow block arrows) defined the shape of the droplet. (For interpretation of the references to colour in this figure legend, the reader is referred to the web version of this article.)

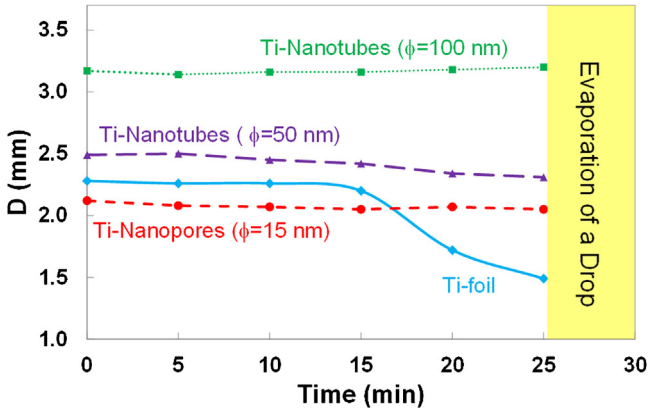

Fig. 4. Time-dependence of contact diameter *D* of various Ti-nanostructures: contact diameter *D* of the droplet (see also Fig. 5) remained practically unaltered for nanorough surfaces whereas it changed considerably for flat Ti-surface.

regime [41], explained later). Due to the liquid penetration, the effective area wetted by water in case of nanorough surfaces is larger than the area of the ideally smooth surface (which equals to $\pi D^2/4$, see Fig. 5). The elevated wetting of the upper part of hollow interiors of the nanopores/nanotubes may result in an increase in attractive and frictional forces, thereby restricting the receding of the droplet edge (contact line) in the lateral direction and keeping the *D* value practically unchanged or minimally changed (Fig. 4). The topographical roughness of the TiO_2 nanostructured surfaces in vertical direction (as shown in Fig. 2) may additionally contribute towards hindrance of the receding droplet, among others due to increased frictional forces.

As evident from Fig. 4, the water droplet contact angle decreases gradually with time during the whole evaporation process in all the presented cases. This phenomenon was observed already in the past, but exclusively on hydrophilic surfaces. The explanation of such behaviour of the contact angle is still not clear [41]. It was further shown that the evaporating water droplet on a hydrophobic surface retains a constant contact angle, while, concomitantly, the contact diameter decreases [41]. On the other hand, the water droplet on a hydrophilic surface initially preserves a constant contact diameter, while the contact angle decreases from the very beginning [41]. Once the receding value of contact is reached, both the contact diameter and the contact angle decrease [41]. In our case (Fig. 4), the nanostructured TiO_2 surfaces behave very differently, as described above. Namely, on nanostructured TiO_2 surfaces the evaporating water droplet preserves/keeps its contact diameter despite of its hydrophobic nature (contact angle > 90°) (Fig. 3b and

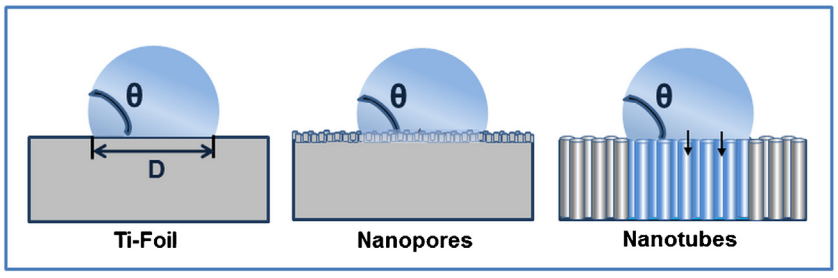

Fig. 5. Schematic diagrams of wetting of Ti-nanostructures: wetting of Ti-foil drives the retraction of the droplet, whereas the nanoporous and nanotubular TiO_2 surfaces are wetted differently by the droplet. Due to changed interfacial forces, the receding of contact area of the drop on Ti O_2-nanostructured surfaces is hampered and thus the contact diameter *D* remains nearby unchanged. (Blue shading is used to indicate aqueous regions whereas arrow depicts the path of wetting nanotube surface). (For interpretation of the references to colour in this figure legend, the reader is referred to the web version of this article.)

c). On the other hand, the contact diameter of the water droplet on Titanium foil recedes during the evaporation process (Fig. 3a).

3.3. Interaction behaviour of water droplet with Ti-nanostructures

According to Wenzel law, the increased roughness of the microstructured surfaces (and thus enhanced effective surface areas) makes the hydrophobic surface even more hydrophobic and hydrophilic surface even more hydrophilic [41]. On the other hand, the contact area of Cassie droplet is determined by the ratio of contact surface area of the drop with the microstructured surface (top surface of protrusions) to the total top surface [41].

Our results indicate that the behaviour of water droplet on the TiO_2 nanoporous and nanotubular surfaces is only partially governed by the Wenzel law or the combined Wenzel–Cassie law [41]. Nevertheless, it is hard to estimate the degree of penetration of the water in the interior of the nanotubes and nanopores and the role of the nanoscale vertical surface roughness. The measured values of the initial contact angle (at time zero) for 15 nm and 50 nm nanotubular surfaces and nanoporous surface (not shown) are larger than the corresponding value for Ti-foil and are increasing from 50 to 15 nm nanotubular surface and further to nanoporous surface. This is not in agreement with the Cassie law, since the top surface (ring) area of the TiO_2 nanotubular surfaces increases following the order from 100, 50 to 15 nm nanotubular surface and finally to nanoporous surface. On the other hand, the initial contact area for 100 nm nanotubular surface appears to be smaller than the initial contact area for Ti-foil surface. Therefore from these contact angle values it cannot be confirmed whether the droplet partially (Wenzel–Cassie droplet) or fully (Cassie droplet) resides on the surface of the nanotubes [41,44].

The wetting phenomenon of Ti-foil can be correlated to the droplet retraction due to the hysteresis of contact angles from slightly rough surfaces [45]. However, the wetting of nanorough surfaces (TiO_2 nanopores or nanotubes), appears to be much more complicated and needs more complex models like Wenzel model [46,47] or Cassie–Baxter model [48] or a combination of them [41]. The nanorough surfaces may act as adsorptive materials at the nanoscale that can wet the interior and the intermediate regions of nanopore/nanotube surfaces, as shown by the schematics in Fig. 5.

3.4. The influence of different diameters of nanotubes on the surface charge

The surface charge of the samples was estimated using the surface streaming potential technique and expressed as the ζ-potential dependence on the pH (Fig. 6). The titanium foil showed its IEP at the most acid pH (pH = 3.74) among the samples. The nanostructured surfaces with nanotubes of 15, 50 and 100 nm in diameter presented their IEP at pH 4.70, 4.58 and 5.18, respectively. The more acidic IEP for titanium foil than for the anodised titanium is partially due to the amorphous oxide structure (short range order), naturally formed by passivation, which may influence the stability and density of the surface hydroxyl groups [25,49,50]. On the other hand, the stoichiometric titanium dioxide nanotubes displayed IEP at more basic pH than titanium. In accordance with Pedimonte et al. [50], a general trend for the nanostructured surfaces was observed, i.e. the IEP became more basic with the increase in pore size. Thus, the nanotube diameters might have an influence on the local surface chemistry at the top-edge of the nanotubes and, consequently, on a different coordination hydroxyl groups, which results in the IEP shift for the 100 nm diameter nanotubular surface. At pH higher than the IEP a negative surface charge exists, therefore at physiological pH all the samples appeared negatively charged. Significant differences in terms of measured ζ-potential values were found:

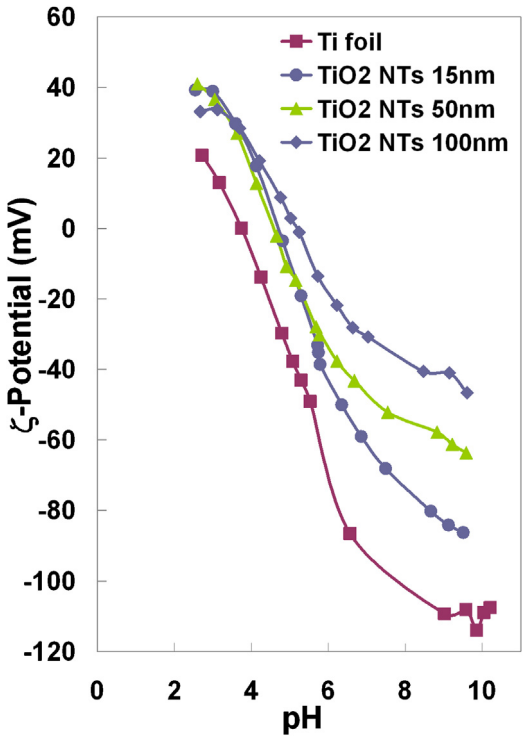

Fig. 6. The pH dependences of ζ-potential for Ti-foil and TiO_2 nanotubular surfaces: ζ-potential for Ti-foil and TiO_2 nanotubular surfaces with 15, 50, and 100 nm diameters as a function of pH in water at 0.001 mol/L concentration of KCl.

the titanium foil showed the highest negative ζ-potential, followed by the series of the nanostructured samples, 15 nm diameter nanotubes, 50 nm diameter nanotubes and 100 nm diameter nanotubes, in sequence. This may be partially explained by increasing top surface (ring) area of TiO_2 nanotubular surface following the order from 100, 50 to 15 nm diameter nanotubes with the highest top surface area. In addition, the total length of the inner and outer edges of the nanotubes (calculated per unit area of the nanotubular surface) is the largest for 15 nm nanotubular surface which may also contribute to more negative (average) surface potential for 15 nm nanotubes (see for explanation Gongadze et al. [18]). Also, an effect of the considerable vertical surface roughness of the 100 nm diameter nanotubes on the average surface charge density cannot be excluded. Among all the samples, the Ti surface covered by 100 nm diameter nanotubes appeared to exhibit at the nanoscale level the most pronounced topographical variation in the vertical direction (see Fig. 2) and also the most hydrophilic character (i.e. the smallest contact angle). Taken all together, the described topographical (Figs. 1 and 2) electrochemical (Fig. 6) features of 100 nm nanotubular surface are proposed to contribute to least negatively charged 100 nm nanotubular surface (having ζ-potential ≈ -35 mV at physiological pH). The observed differences in ζ-potential and IEP values between different diameter nanotubular surfaces clearly indicate the important influence of nanotubes' diameter and vertical topographical variation (roughness) on the electrochemical properties of TiO_2 nanotubular surfaces.

4. Conclusions

We have successfully fabricated well-defined titanium-nanorough surfaces using electrochemical anodisation by a systematic optimisation of the experimental conditions. The titanium dioxide nanorough surfaces demonstrably hinder the receding of the contact area during the evaporation of water droplet. The exposure of much larger effective (real) surface area

and the consequent wettability of the nanorough surfaces, as compared to micro- and macroscopically rough ones, are potentially advantageous properties while developing biomedical implants [51–53]. Moreover, the predicted behaviour of nanorough surfaces, with regards to the suppression of receding of contact area, could further contribute towards an improved biological response in terms of adhesion of proteins, membranous components and cells to the implant surfaces [14,18,54,55]. The larger effective (real) surface area of the implant generated by the nanostructuring of its surface is expected to improve the bone-to-implant contact, which is one of the important elements for the success of orthopaedic implants.

Acknowledgements

The authors would like to acknowledge Slovenian Research Agency (ARRS) grants No. P2-0232, P3-0388, J1-6728 for the financial support. The authors are grateful to Anca Mazare for SEM figures (Fig. 1).

References

[1] P. Roy, S. Berger, P. Schmuki, Angew. Chem. Int. Ed. Engl. 50 (2011) 2904.
[2] C.N. Elias, J.H.C. Lima, R. Valiev, M.A. Meyers, JOM 60 (2008) 46.
[3] D.F. Williams, Biomaterials 29 (2008) 2941.
[4] S. Anil, P.S. Anand, H. Alghamdi, J.A. Jansen, in: I. Turkyilmaz (Ed.), Implant Dentistry – A Rapidly Evolving Practice, InTech, Rijeka, 2011, p. 83.
[5] A. Popelka, I. Novak, M. Lehocky, M. Spirkova, F. Bilek, Molecules 17 (2012) 762.
[6] J.L. Garcia, J. Pachernik, M. Lehocky, P. Humpolicek, P. Saha, Prog. Colloid Polymer Sci. 138 (2010) 89.
[7] M. Ventre, F. Causa, P.A. Netti, J. R. Soc. Interface 9 (2012) 2017.
[8] Y. Tamada, Y. Ikada, J. Colloid Interface Sci. 155 (1993) 155.
[9] L.C. Siedlecki, A. Christopher, Biomaterials 28 (2007) 3273.
[10] G. Sigal, M. Mrksich, G. Whitesides, J. Am. Chem. Soc. 120 (1998) 3464.
[11] T. Akkas, C. Citak, A. Sirkecioglu, F. Seniha Guner, Polymer Int. 62 (2013) 1202.
[12] E. Gongadze, A. Velikonja, Š. Perutkova, P. Kramar, A. Maček-Lebar, V. Kralj-Iglič, A. Iglič, Electrochim. Acta 126 (2014) 42.
[13] Application note 17: influence of topography and wettability on biocompatibility. <http://www.biolinscientific.com/zafepress.php?url=%2Fpdf%2FAttension%2FApplication%20Notes%2FAT_AN_17_roughbio.pdf>.
[14] M. Kulkarni, A. Flašker, M. Lokar, K. Mrak-Poljšak, A. Mazare, A. Artenjak, S. Čučnik, S. Kralj, A. Velikonja, P. Schmuki, V. Kralj-Iglič, S. Sodin-Semrl, A. Iglič, Int. J. Nanomed. 10 (2015) 1359.
[15] K.C. Popat, L. Leoni, C.A. Grimes, T.A. Desai, Biomaterials 28 (2007) 3188.
[16] S. Bauer, J. Park, K.V.D. Mark, P. Schmuki, Acta Biomater. 4 (2008) 1576.
[17] M. Kulkarni, A. Mazare, E. Gongadze, Š. Perutkova, V. Kralj-Iglič, I. Milošev, P. Schmuki, A. Iglič, M. Mozetič, Nanotechnology 26 (2015) 062002.
[18] E. Gongadze, D. Kabaso, S. Bauer, S.T. Slivnik, P. Schmuki, U. van Rienen, A. Iglič, Int. J. Nanomed. 6 (2011) 1801.
[19] P. Roach, D. Englin, K. Rohde, C.C. Perry, J. Mater. Sci. Mater. Med. 18 (2007) 1263.
[20] A.J. García, in: C. Werner (Ed.), Polymer Regenerative Medicine, vol. 203, Springer, Berlin, Heidelberg, 2006, p. 171.
[21] M. Lotfi, M. Nejib, M. Naceur, in: Rosario Pignatello (Ed.), Advances in Biomaterials Science and Biomedical Applications, InTech, Rijeka, 2013, p. 207, http://dx.doi.org/10.5772/53542, ISBN: 978-953-51-1051-4.
[22] K.C. Hazen, D.L. Brawner, M.H. Riesselman, M.A. Jutila, J.E. Cutler, Infect. Immun. 59 (1991) 907.
[23] A. Kongde, T. Bechtold, L. Teufel, J. Appl. Polymer Sci. 96 (2005) 1421.
[24] F. Fang, J. Satulovsky, I. Szleifer, Biophys. J. 89 (2005) 1516.
[25] M. Textor, C. Sittig, V. Frauchiger, S. Tosatti, D. Brunette, in: D. Brunette, P. Tengvall, M. Textor, P. Thomsen (Eds.), Titanium in Medicine, Springer Verlag, Heidelberg and Berlin, 2001, p. 171.
[26] R.E. Baier, J. Mater. Sci. Mater. Med. 17 (2006) 1057.
[27] B. Boyan, D. Dean, C. Lohmann, D. Cochran, V. Sylvia, Z. Schwartz, in: D. Brunette, P. Tengvall, M. Textor, P. Thomsen (Eds.), Titanium in Medicine, vol. 17, Springer Verlag, Heidelberg and Berlin, 2001, p. 561.
[28] W.A. Soskolne, S. Cohen, L. Sennerby, A. Wennerberg, L. Shapira, Clin. Oral Implant Res. 13 (2002) 86.
[29] L. Bozec, G. van der Heijden, M. Horton, Biophys. J. 92 (2007) 70.
[30] G.A. Abrams, S.S. Schaus, S.L. Goodman, P.F. Nealey, C.J. Murphy, Cornea 19 (2000) 57.
[31] L. Bozec, M. Horton, Biophys. J. 88 (2005) 4223.
[32] K.L. Mittal (Ed.), Contact Angle, Wettability and Adhesion, vol. 4, CRC Press, Utrecht, 2006.
[33] R. Kane, P.X. Ma, Mater. Today 16 (2013) 11.
[34] L. Zhang, T.J. Webster, Nano Today 4 (2009) 66.
[35] E. Engel, A. Michiardi, M. Navarro, D. Lacroix, J.A. Planell, Trends Biotechnol. 26 (2008) 39.
[36] A. Curtis, C. Wilkinson, Biomaterials 18 (1997) 1573.
[37] J.Y. Lim, H.J. Donahue, Tissue Eng. 13 (2007) 1879.
[38] E. Gongadze, D. Kabaso, S. Bauer, J. Park, P. Schmuki, A. Iglič, Mini-Rev. Med. Chem. 13 (2013) 94.
[39] D. Kowalski, D. Kim, P. Schmuki, Nano Today 8 (2013) 235.
[40] D.H. Shin, T. Shokuhfar, C.K. Choi, S.H. Lee, C. Friedrich, Nanotechnology 22 (2011) 315704.
[41] J. Berthier, K.A. Brakke, The Physics of Microdroplets, Scrivener Publishing, Massachusetts, 2012, pp. 201.
[42] N. Verplanck, Y. Coffinier, V. Thomy, R. Boukherroub, Nanoscale Res. Lett. 2 (2007) 577.
[43] Z. Zhou, F. Li, Q. Song, T. Yi, X. Hou, C. Huang, Chem. Lett. 34 (2005) 1298.
[44] D. Quéré, Nat. Mater. 1 (2002) 14.
[45] R.J. Good, J. Adhes. Sci. Technol. 6 (1992) 1269.
[46] R.N. Wenzel, Ind. Eng. Chem. 28 (1936) 988.
[47] R.N. Wenzel, J. Phys. Colloid Chem. 53 (1949) 1466.
[48] A.B.D. Cassie, S. Baxter, Trans. Faraday Soc. 40 (1944) 546.
[49] S. Roessler, R. Zimmermann, D. Scharnweber, C. Werner, H. Worch, Colloid Surf. B: Biointerface 26 (2002) 387.
[50] B.J. Pedimonte, T. Moest, T. Luxbacher, C. von Wilmowsky, T. Fey, K.A. Schlegel, P. Greil, Acta Biomater. 10 (2014) 968.
[51] E. Ogorevc, V. Kralj-Iglic, P. Veranic, Radiol. Oncol. 47 (2013) 197.
[52] N. Recek, M. Mozetic, M. Jaganjac, L. Milkovic, N. Zarkovic, A. Vesel, Vacuum 98 (2013) 116.
[53] A. Vesel, K. Elersic, M. Modic, I. Junkar, M. Mozetic, Materials 7 (2014) 2014.
[54] V. Kralj-Iglic, Int. J. Nanomed. 7 (2012) 3596.
[55] M. Jaganjac, A. Vesel, L. Milkovic, N. Racek, M. Kolar, N. Zarkovic, A. Latiff, K.S. Karin-Kleinschek, M. Mozetic, J. Biomed. Mater. Res. A 102 (2014) 2305.